Modeling molecular transport in slit pores

Owen G. Jepps, Suresh K. Bhatia, and Debra J. Searles

Citation: The Journal of Chemical Physics **120**, 5396 (2004); doi: 10.1063/1.1647516

View online: http://dx.doi.org/10.1063/1.1647516

View Table of Contents: http://scitation.aip.org/content/aip/journal/jcp/120/11?ver=pdfcov

Published by the AIP Publishing

Modeling molecular transport in slit pores

Owen G. Jepps and Suresh K. Bhatia[a)]
Division of Chemical Engineering, The University of Queensland, Brisbane, QLD 4072, Australia

Debra J. Searles
School of Science, Griffith University, Brisbane QLD 4111, Australia

(Received 8 September 2003; accepted 18 December 2003)

We examine the transport of methane in microporous carbon by performing equilibrium and nonequilibrium molecular dynamics simulations over a range of pore sizes, densities, and temperatures. We interpret these simulation results using two models of the transport process. At low densities, we consider a molecular flow model, in which intermolecular interactions are neglected, and find excellent agreement between transport diffusion coefficients determined from simulation, and those predicted by the model. Simulation results indicate that the model can be applied up to fluid densities of the order to 0.1–1 nm^{-3}. Above these densities, we consider a slip flow model, combining hydrodynamic theory with a slip condition at the solid–fluid interface. As the diffusion coefficient at low densities can be accurately determined by the molecular flow model, we also consider a model where the slip condition is supplied by the molecular flow model. We find that both density-dependent models provide a useful means of estimating the transport coefficient that compares well with simulation. © *2004 American Institute of Physics.* [DOI: 10.1063/1.1647516]

I. INTRODUCTION

Many of the various applications of microporous materials, such as catalysis and species separation, involve the transport of adsorbed fluids. Consequently, a capacity to determine the transport properties of these materials provides a considerable advantage for the continuing development of further applications. The development of models of transport in confined regions has a long history. Early experimental and theoretical work by Knudsen[1] and Smoluchowski[2] established a description of the pressure-driven flow of rarefied gases in cylindrical tubes. For systems undergoing molecular flow, where the Knudsen number $Kn>1$ ($Kn=\lambda/H$ is the ratio of the mean-free path λ of molecules to the characteristic container dimension H, such as the tube radius or pore width), transport is dominated by collisions between molecules and the wall, and the transport coefficient is independent of Kn. At $Kn<0.01$, the Navier–Stokes equations can be applied to provide a continuum, or viscous model for the (Poiseuille) transport flow. The continuum model can be augmented with a slip boundary condition determined from momentum balance, which extends its applicability to the range $Kn<0.1$.[3] However, there is a range—the so-called transition region,[3] corresponding approximately to $0.1<Kn<1$—where none of the aforementioned models can be applied.[3,4] Other models have been subsequently developed to bridge the transition region, include kinetic theory models that explicitly addressed both wall collisions and intermolecular collisions,[5,6] and solutions to the Boltzmann equation.[7,8]

These models were developed for systems where the molecular radius was typically much smaller than the container dimension, and thus where hard-wall (and often hard-sphere) approximations are appropriate. However, when one considers transport in microporous media, where the molecular and pore dimensions are of similar orders of magnitude, the nature of the fluid–fluid and solid–fluid interactions becomes much more significant, and must be incorporated into any successful model of transport on this scale. Needless to say, the incorporation of these elements in a general theory is far from trivial. Rigorous theories for general intermolecular interactions based on the platform of Enskog theory have been derived in this vein[9,10]—however, their application to transport in micropores is difficult and computationally expensive. An alternative means of accounting for intermolecular interactions is the augmentation of the hydrodynamic theory with a locally-averaged density model (LADM).[11] Such a model is analogous to the viscous model of the classical hard-sphere hard-wall theory, and therefore we might anticipate that diffuse transport in microporous media would also admit a slip model and a molecular flow model. Indeed, slipping at the solid–fluid interface on microscopic scales has been identified in both experimental work[12,13] and simulation,[14,15] and recent work in this laboratory has focused on the development of a slip model which can be used to predict transport coefficients in micropores. The slip model[16,17] was consistent with simulation data over densities ranging down to the molecular flow region, and the authors observed an increase in the collision rate of fluid molecules at the wall that was consistent with the transition from slip to purely viscous flow at higher densities.

Molecular simulation plays an important role in the development of theories of transport in confined fluids, facilitating study of the behavior at the microscopic level.[18–21] In this paper, we shall use molecular dynamics (MD) techniques to generate values of the transport diffusion coefficient, against which we can test our theory. Recent studies

a)Author to whom correspondence may be addressed. Electronic mail: sureshb@cheque.uq.edu.au.

have focused on three techniques for the estimation of transport diffusion coefficients—equilibrium molecular dynamics (EMD), forced-flow nonequilibrium molecular dynamics (NEMD), and dual control-volume grand canonical molecular dynamics (DCV).[22–24] This final technique has been developed to examine the nature of transport during diffusive processes, by introducing explicit chemical potential gradients into the system. Recent results[16,17,25] suggest that the transport coefficients measured by these three techniques coincide. In light of the technical difficulty and computational intensity in implementing DCV, we will use EMD and NEMD in order to measure the transport coefficients.

In the current work, we consider the development of models to describe transport in slit micropores. We develop a theory for transport in the molecular flow regime. The approach is analogous to that used to derive the well-known Knudsen formula—we consider molecules being driven along the pore, undergoing diffuse reflections at the boundary. In the molecular flow limit, we neglect intermolecular interactions. However, a significant departure from the Knudsen expression arises due to the interaction between fluid molecules and the pore, which is represented by a continuous one-dimensional potential across the pore and the diffuse boundary conditions. We note here an early attempt to compute the flux for transport due to a concentration gradient, where trajectories were obtained numerically.[26] However, here we consider the molecules as oscillators in an external field, and treat the trajectories analytically, with a more precise relation between the transport coefficient and the trajectory characteristics. We find excellent agreement between this model and molecular dynamics simulation in the molecular flow regime.

We also consider models for the transport at higher densities, where intermolecular interactions cannot be neglected. At higher densities, therefore, we determine estimates for the transport coefficient of methane in the graphitic slit pore via the slip model recently developed in our laboratory,[16,17] which we call model A. We also consider a model where the density-dependence of the transport coefficient is estimated by the viscous contribution determined from the slip model, and the oscillator model is used to provide the low-density limit, which we call model B. We find that both models can be used to estimate the density dependence of the transport coefficient in micropores.

II. THEORY

A. Oscillator model

The transport of molecules in micropores is generally understood to proceed via diffusion.[27] For the single species case, the driving force can therefore be considered equivalently as either a chemical potential gradient, or a pressure gradient, related by the Gibbs–Duhem equation. The boundary conditions at the solid–fluid interface play a crucial role in the determination of the transport coefficient in single-species adsorption—at equilibrium, they alone determine the dynamics of the fluid center-of-mass fluctuations at the microscopic level, and therefore the collective transport properties.

Theories describing transport processes in the molecular flow regime have generally been formulated under conditions of pressure-driven flow, where a density gradient is maintained along the length of a confined region. This leads to a transport process where the driving force of the pressure gradient is balanced by momentum exchange at the boundary. Commonly, this momentum exchange is expressed in the form of diffuse boundary conditions—under these conditions, when a molecule is at its point of nearest approach to the wall, the component of its momentum parallel to the pore walls is randomly reoriented. The difference in pressures at either end of the confined region, required to generate the pressure gradient, constitutes a thermodynamic boundary condition. In the development of molecular simulation methodologies, it has been noted that thermodynamic boundary conditions can often be replaced by fictitious external forces, which yield the same transport coefficients (and are generally easier to implement in simulation).[28] We take advantage of this duality in the development of our theoretical model, by considering a molecular flow transport process that is driven by an external force field, rather than by a pressure gradient.

Let us consider a system of fluid molecules driven along a slit pore, at temperature T. We describe the slit pore in Cartesian coordinates, with the pore walls represented by infinite planes normal to the x axis and the pore axis lying in the z direction. The pore walls are separated by a distance H. At sufficiently low densities, we can safely neglect intermolecular interactions, considering only the solid–fluid interaction and the external field.

The solid–fluid interaction consists of z momentum exchange between fluid molecules and the solid wall, and a force field normal to the wall, described by a continuous potential $V(x)$. We represent this force field using the Steele 10-4-3 potential[29] for each wall. Assuming the pore to be symmetric, we observe two different forms of $V(x)$—for $H < H_c$ (for some critical pore width H_c, dependent on the fluid and solid molecular radii) there is a single minimum at the pore center ($x=0$ hereafter), while for $H>H_c$ there are two local minima (at $x=\pm x_0$), separated by a local maximum at the pore center (see Fig. 1). In these wider pores, we define the region bounded by the potential minima as the ''bounded'' region [corresponding to the striped region in Fig. 1(b)], and the rest of the pore as the ''repulsive'' region [the dotted regions in Fig. 1(b)]. In the narrow pores, the entire pore can be considered as a ''repulsive'' region. While the model that we develop can be extended beyond these restrictions, in the current context we will only consider potentials $V(x)$ as described above.

An interaction potential of the form $V(x)$ precludes the exchange of z momentum between molecules and the pore, which is an essential part of the transport dynamics. We therefore introduce the following random boundary condition—when a molecule turns away from a wall in the repulsive region, it loses all of its z momentum on average. The specific nature of the boundary condition, beyond this condition, is not needed for the model. We note that the diffuse boundary condition satisfies this condition.

The thermodynamic mechanism driving the transport process is represented by an external force field of magnitude

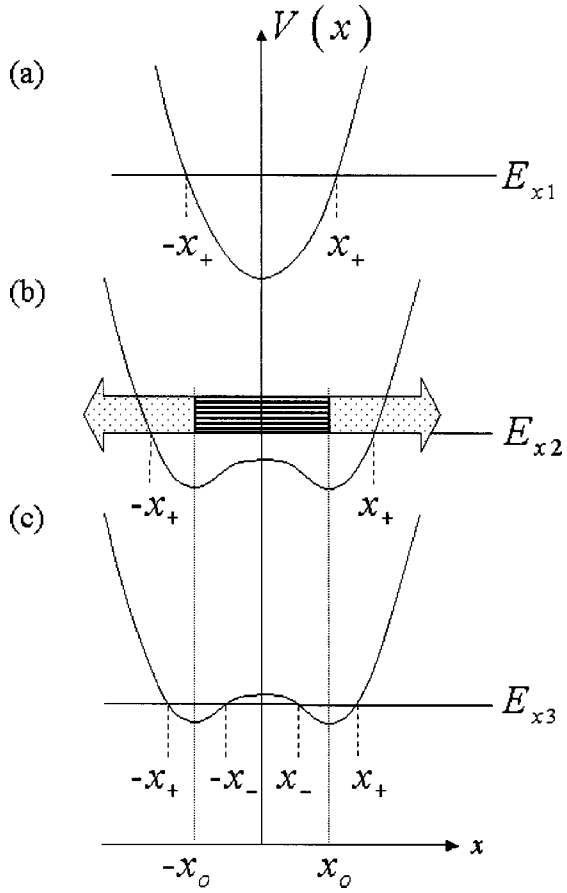

FIG. 1. The range of oscillation of a molecule is determined by the solid–fluid interaction potential $V(x)$, and by E_x. In (a) and (b), the molecule has sufficient energy to cross the pore center, and the oscillation is bounded by $\pm x_+$. In (c) it cannot cross the pore center, and oscillates in one of two regions. In the double-minimum pore, we define a bounded region between the potential minima $\pm x_0$, corresponding to the striped region in (b). We also define a repulsive region, corresponding to the dotted regions in (b).

F in the positive z direction, applied to each molecule. The transport diffusivity D_0 is related to the entropy production, and given by the expression[30]

$$D_0 = Jk_BT/\rho F = \langle v_z \rangle k_BT/F, \tag{1}$$

where $\langle v_z \rangle$ is the average z velocity across the pore, and k_B is the Boltzmann constant. To calculate D_0, we must determine $\langle v_z \rangle$ from the model.

Ignoring fluid–fluid interactions, the dynamics of a single molecule can be determined from the Hamiltonian

$$H = V(x) - Fz + p_x^2/2m + p_y^2/2m + p_z^2/2m,$$

noting that ''reflections'' with the pore introduce discontinuities in both p_y and p_z (hereafter, we will refer to interactions between fluid molecules as ''collisions,'' and interactions between a fluid molecule and the pore wall as ''reflections''). We note that

$$E_x = V(x) + p_x^2/2m, \quad E_y = p_y^2/2m,$$

$$E_z = -Fz + p_z^2/2m,$$

are constant between reflections, and that E_x is constant throughout. The motion in the x direction will therefore be periodic. In a single-minimum pore, a molecule would oscillate between $\pm x_+$, where x_+ is the upper bound of the oscillation [Fig. 1(a)]. In a double-minimum pore, a molecule either oscillates across the pore center [between bounds $\pm x_+$, as in Fig. 1(b)], or within bounds $x_- < x_+$ of the same sign [Fig. 1(c)]. Without loss of generality, we assume these bounds to be positive. In all cases, x_+ is in the repulsive region, and completely determines the oscillatory behavior. A molecule passes through any point x along its trajectory twice—once at a time t_x *after* a reflection, and later at time t_x *before* a reflection. In a symmetric pore, the period between successive collisions τ will be a continuous function of x_+, and therefore of E_x. If the molecule leaves a reflection with random z momentum p_i, such that $\langle p_i \rangle = 0$, then the average z momentum of a molecule at x will be

$$\tfrac{1}{2}(\langle p_i + Ft_x \rangle + \langle p_j + F[\tau(E_x) - t_x] \rangle) = F\tau(E_x)/2,$$

(where $p_i = p_j$ if the molecule does not have sufficient energy to traverse the whole pore). We note that this result is independent of x. The solid–fluid interaction, together with the external force, induce molecules to oscillate across the pore, with mean z velocity $v_z = F\tau(E_x)/2m$.

In the real fluid, two molecules will eventually collide. The time over which they interact will be small, compared with the time between collisions. Consequently, the main contribution of the collision to the overall transport will be to change the values of E_x for each molecule. The fluid–fluid interactions in the real fluid therefore perform a mixing role, redistributing the E_x among fluid molecules in accordance with the canonical distribution. Therefore, we represent the real fluid–fluid interaction in our model by invoking the canonical ensemble to describe the distribution of E_x among fluid molecules.

Using the canonical distribution together with our definition for the diffusion coefficient Eq. (1), we determine that

$$D_0 = \frac{k_BT}{F}\langle v_z \rangle = \frac{k_BT}{2m}\frac{\int_{-\infty}^{\infty}\int_{-H/2}^{H/2}\tau(E_x(x,p_x))e^{-E_x(x,p_x)/k_BT}dxdp_x}{\int_{-\infty}^{\infty}\int_{-H/2}^{H/2}e^{-E_x(x,p_x)/k_BT}dxdp_x}, \tag{2}$$

where $x \in [-H/2, H/2]$ ranges over the entire pore. We note that this expression for D_0 is equivalent to the self-diffusion coefficient, a result we anticipate in a system where the momenta of different molecules are uncorrelated in the absence of fluid–fluid interactions.

All that remains is to determine $\tau(E_x)$, which we obtain by rearranging the definition of E_x,

$$\tau(E_x) = \sqrt{2m}\int_{x_-(E_x)}^{x_+(E_x)}[E_x - V(x)]^{-1/2}dx. \tag{3}$$

While we have developed the oscillator model here with the diffuse boundary condition in mind, we note that the only property of the boundary condition that we have used is that molecules return to the system with average zero momentum in the z direction. It is therefore possible to extend this model, formulating expressions for D_0 based on alternative boundary conditions.

A common alternative to diffuse boundary conditions, used as early as Maxwell to explain slip flow,[31] incorporates a degree of specular reflection. Under these conditions, a fraction α of molecular reflections at the wall are diffuse, with the remaining fraction $(1-\alpha)$ being specular. In this case, D_0 becomes a function of α, where the coefficient D_0 as determined by Eq. (2) above corresponds to the fully diffuse case, $D_0(\alpha)|_{\alpha=1}$. If $0<\alpha<1$, then the trajectory of a molecule with energy E_x consists of a random sequence of specular and diffuse reflections. The probability of observing n consecutive specular reflections between successive diffuse reflections is $(1-\alpha)^n\alpha$, for any non-negative integer n, and the time over which the molecule gains momentum from the external field is $(n+1)\tau(E_x)$. It follows that the mean z velocity of such a molecule in the pore is given by

$$\begin{aligned}\overline{v_z}(E_x) &= \frac{\int v_z(t)dt}{\int dt} \\ &= \frac{\Sigma_{n=0}^{\infty}\alpha(1-\alpha)^n F[(n+1)\tau(E_x)]^2/(2m)}{\Sigma_{n=0}^{\infty}\alpha(1-\alpha)^n[(n+1)\tau(E_x)]} \\ &= \frac{F\tau(E_x)}{2m}\frac{\Sigma_{n=0}^{\infty}(1-\alpha)^n(n+1)^2}{\Sigma_{n=0}^{\infty}(1-\alpha)^n(n+1)} \\ &= \frac{F\tau(E_x)}{2m}\frac{(2-\alpha)}{\alpha}\end{aligned}$$

and the transport diffusion would be given by the relation

$$\begin{aligned}D_0(\alpha) &= \frac{k_BT}{F}\langle v_z\rangle \\ &= \frac{(2-\alpha)}{\alpha}\frac{k_BT}{2m} \\ &\quad\times\frac{\int_{-\infty}^{\infty}\int_{-H/2}^{H/2}\tau(E_x(x,p_x))e^{-E_x(x,p_x)/k_BT}dxdp_x}{\int_{-\infty}^{\infty}\int_{-H/2}^{H/2}e^{-E_x(x,p_x)/k_BT}dxdp_x}\end{aligned}$$

with $\tau(E_x)$ evaluated as before [via Eq. (3)]. We note that this is consistent with the Smoluckowski's extension of Knudsen's result for the Maxwell boundary condition,[2] and extends our early results with the oscillator model.[32]

B. Viscous models

As the density of our system increases, it is no longer tenable to consider the fluid–fluid interactions as merely mixing the energy distribution of the molecules. Such interactions will alter the nature of the momentum exchange between fluid and pore. At moderate densities, the path of the molecule will change, thereby perturbing the period of oscillation and the momentum exchange. At higher densities, the oscillator model no longer captures the essential behavior of diffusing molecules—molecular motion normal to the walls will be restricted by intermolecular interactions, and viscous effects will change the streaming behavior of molecules exchanging momentum with the walls.

Consequently, we must turn to alternative methods in order to predict transport properties. Recent work in our laboratory has focused on a hydrodynamic slip model describing the density dependence of the transport coefficient, which gave good agreement with simulation data obtained for methane transport in cylindrical silica pores.[16,17]

The slip model is developed in the context of a transport process driven by an external force, rather than by a pressure gradient, with system properties varying as a function of position x across the pore only. An expression for the flux of the fluid through the pore is developed, which is then substituted into Eq. (1) to determine the transport coefficient. The flux is determined from the product of density and velocity profiles of the absorbed fluid across the pore. The density profile can be obtained from an appropriate density functional theory, or (as in our case) from molecular simulation, and the velocity profile from the Navier–Stokes relation

$$\frac{d}{dx}\left(\eta(x)\frac{d}{dx}v_z(x)\right) = -F(x)\rho(x), \tag{4}$$

where $\rho(x)$, $v_z(x)$, $\eta(x)$, and $F(x)$ represent the density, velocity, and viscosity profiles, and the mean external force at x. The viscosity profile can be estimated using the (equilibrium) correlation of Chung *et al.*,[33] which gives the viscosity as a function *inter alia* of the density. The density used for this correlation is not the local density $\rho(x)$, but a locally averaged density, as proposed by Bitsanis *et al.*[11] In the bounded region inside the pore, $F(x)\equiv F$, the constant external force driving the transport. Consequently, we can solve the second-order equation for $v_z(x)$ in this region. The two boundary conditions are provided by imposing symmetry across the pore, and by introducing a frictional boundary condition of the form[16,17]

$$k\rho_0 v_z(x_0) = mv_z(x_0)Z_0 = -\eta(x_0)\left.\frac{dv_z(x)}{dx}\right|_{x=x_0}, \tag{5}$$

where Z_0 represents the frequency of reflections at the pore wall, determined from kinetic theory. Integration of Eq. (4) leads to

$$v_z(x) = \frac{F}{k\rho_0}\int_{-x_0}^{0}\rho(\xi)d\xi + \int_{-x_0}^{x}\frac{F}{\eta(\xi)}\int_{\xi}^{0}\rho(\zeta)d\zeta d\xi \tag{6}$$

if $x\in[-x_0,x_0]$ is restricted to the bounded region where $F(x)$ is constant. The first term on the right-hand side of Eq. (6) is the constant boundary term $v_z(x_0)$. The second term describes the effect of the fluid viscosity on the velocity profile. The transport diffusion coefficient is therefore given by

$$\begin{aligned}D_0 &= \frac{k_BT}{\hat{\rho}FH}\int_{-x_0}^{x_0}\rho(x)v_z(x)dx \\ &= \frac{2k_BT}{\hat{\rho}H}\left[\frac{1}{k\rho_0}\left(\int_{-x_0}^{0}\rho(\xi)d\xi\right)^2 \right. \\ &\quad \left. + \int_{-x_0}^{0}\frac{1}{\eta(\xi)}\left(\int_{\xi}^{0}\rho(\xi)d\xi\right)^2 dx\right].\end{aligned} \tag{7}$$

We shall refer to the model represented by Eq. (7) for the transport coefficient as model A. We note that model A consists of a boundary term, and a viscous term which goes to zero in the low-density (molecular flow) limit. The boundary term should therefore converge to the oscillator model

estimates for the diffusion coefficient in the low density limit. We therefore propose a further expression for the transport coefficient, given by

$$D_0 = D_0^{\mathrm{OSC}} + \frac{2k_BT}{\hat{\rho}H}\int_{-x_0}^{0}\frac{1}{\eta(\xi)}\left(\int_{\xi}^{0}\rho(\xi)d\xi\right)^2 dx, \qquad (8)$$

where D_0^{OSC} is the oscillator model transport coefficient, given by Eq. (2). This model we denote model B. In Sec. IV we explore these two models through molecular dynamics simulation. The application of these approaches to cylindrical nanopores has recently also been investigated.[34]

III. SIMULATION DETAILS

In this paper, we apply the theory developed in the previous section to the transport of methane in carbon slit micropores, with pore widths $H \leqslant 2$ nm. In the simulations, methane molecules were represented as spherically symmetric, interacting with one another through a Lennard-Jones (LJ) 12-6 potential. The LJ parameters for methane were chosen to be $\epsilon_f/k_B = 148.1$ K, $\sigma_f = 0.381$ nm. Fluid–fluid interactions were cut off at a radius of $1.5\,\mathrm{nm} \approx 4\sigma_f$. Each slit pore wall was represented by a Steele 10-4-3 potential,[29] with LJ parameters defined via the Lorentz–Berthelot combining rules, where $\epsilon_s/k_B = 28.0$ K, $\sigma_s = 0.340$ nm for carbon.

Grand canonical Monte Carlo (GCMC) simulations were used to generate starting configurations for the MD simulations at various densities, as well as to generate accurate equilibrium density profiles. System dimensions were chosen to ensure that the mean number of molecules produced was approximately 500, and the simulations were run for the order of 10^8 Monte Carlo steps, to ensure sufficient convergence of the density profiles.

In order to determine values of D_0, both EMD and NEMD methods were utilized to simulate an NVT system. To control the system temperature, a Gaussian thermostat was introduced,[28] with equations of motion

$$\dot{\mathbf{r}}_i = \mathbf{p}_i/m,$$

$$\dot{\mathbf{p}}_i = \frac{\partial V}{\partial \mathbf{r}_i} + \mathbf{F}^{\mathrm{ext}} + \alpha(t)\mathbf{p}_i',$$

where $\mathbf{r}_i$, $\mathbf{p}_i$ represent the positions and momenta of the fluid molecules, V is the combined solid–fluid and fluid–fluid interaction potential, $\mathbf{F}^{\mathrm{ext}}$ is an applied external field (set to zero for EMD), and $\alpha(t)$ is the thermostat multiplier, acting on the peculiar momenta $\mathbf{p}_i'$, which were calculated by determining the molecular momenta in the reference frame of the fluid's center of mass. These equations were solved using a fifth-order Gear predictor–corrector integrator, with a time step of 1–2 fs. In order to permit momentum exchange between the solid and the fluid parallel to the walls, diffuse boundary conditions were applied.[35] Data were obtained by averaging results from runs of length 2×10^6 time steps, each beginning from distinct initial conditions. For each run, averages were collected only after the system had been allowed to relax to equilibrium or the steady state (over approximately 40 000 time steps).

Values of D_0 were determined using both EMD and NEMD. In the EMD simulations, values of D_0 were determined using the Green–Kubo relation between the transport diffusion coefficient and the autocorrelation of the fluid's center-of-mass motion along the pore axis,

$$D_0 = \frac{1}{N}\lim_{\tau\to\infty}\int_0^{\tau}\left\langle \sum_i \sum_j v_{zi}(0)v_{zj}(t)\right\rangle dt.$$

For the NEMD simulations, an external acceleration in the range of 0.01–0.04 $\mathrm{nm\,ps^{-2}}$ was applied in the positive z direction. The range of forces was chosen such that a reasonable signal to noise ratio was observed, without driving the system beyond linear response. The values of D_0 were obtained from the flux J measured during the simulation, in accordance with Eq. (1),

$$D_0 = Jk_BT/\hat{\rho}F^{\mathrm{ext}},$$

where $\hat{\rho}$ is the mean fluid density in the pore.

IV. RESULTS AND DISCUSSION

A. Simulation results

GCMC simulations were performed in pores of width $H = 1.0$ nm, 1.4 nm, and 2.0 nm, at temperatures $T = 298$ K, 350 K, and 400 K, over a range of densities. Typical density profiles are shown in Fig. 2. We note the two strong peaks in all cases, in the vicinity of the solid–fluid potential minima. In all pores at low density, fluid molecules occupy the two planes near these minima. Two basic trends are observed in the variation of the density profile with increasing total density. In the narrowest pore, the solid–fluid potential minima are within σ_f of one another, and the balance between the repulsive force from one wall and the repulsive interaction with molecules near the opposite wall drives the two density peaks further apart. In the wider pores, the potential minima are wide enough to accommodate one, or two, layers of fluid molecules between them, and the positions of the density peaks remain almost constant over the densities observed.

Using GCMC configurations as initial conditions, molecular dynamics simulations were then performed in order to determine transport coefficients over the same range of pore widths and temperatures. As has been observed previously,[16,17] the density profiles from GCMC, EMD, and NEMD agreed with one another for all systems examined. Figure 3 depicts this agreement in the 2.0 nm pore at 400 K, at high density, and is typical of the agreement observed.

The transport coefficients determined from the EMD and NEMD simulations were in good agreement with one another. This agreement is anticipated from recent results obtained using identical boundary conditions in cylindrical pores[17] and atomistic boundaries.[25] Figure 4 shows the variation of the transport coefficient with pore density in the three pore widths considered at 298 K. At low densities, corresponding to the Henry's law region, the transport coefficients remain constant. As with the density profiles, we observe two different trends in the variation of transport coefficient with pore density beyond the Henry's law regime. In the 1.0 nm pore, the transport coefficient decreases with increasing pore

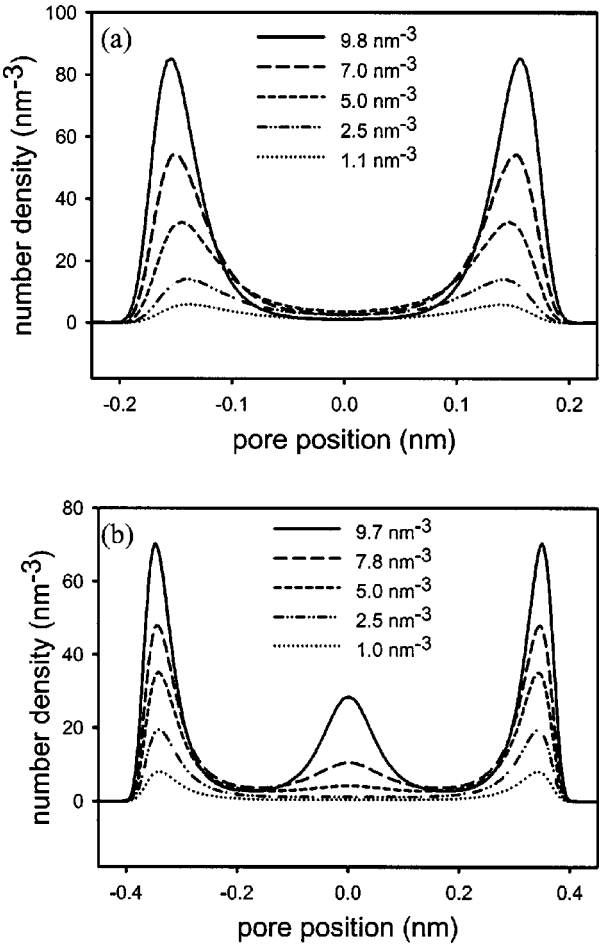

FIG. 2. Density profiles at equilibrium for methane in carbon slit micropores of width (a) 1.0 nm and (b) 1.4 nm at 298 K, at various mean fluid densities.

density. In the wider pores, the transport coefficient increases as the fluid density increases beyond the Henry's law regime, until an upper bound is reached. Strong dependence on the pore size of the relation between the transport coefficient and the density has been observed previously.[18]

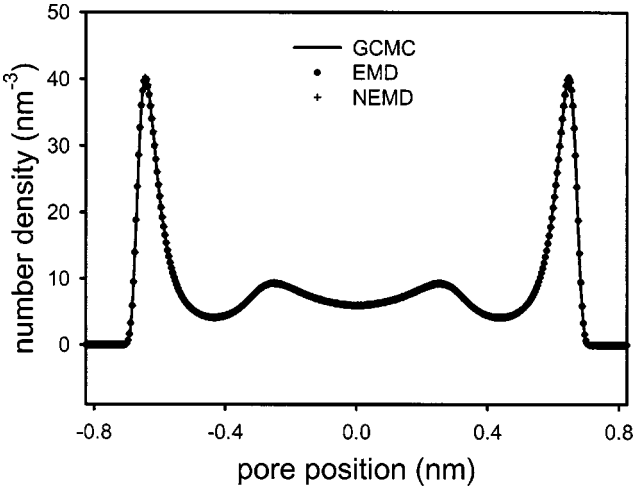

FIG. 3. Density profiles obtained from GCMC (solid line), EMD (dots), and NEMD (crosses) simulations of methane in a carbon slit micropore of width 2.0 nm at 400 K, at a mean density of $\hat{\rho}=6.9339\ \mathrm{nm}^{-3}$.

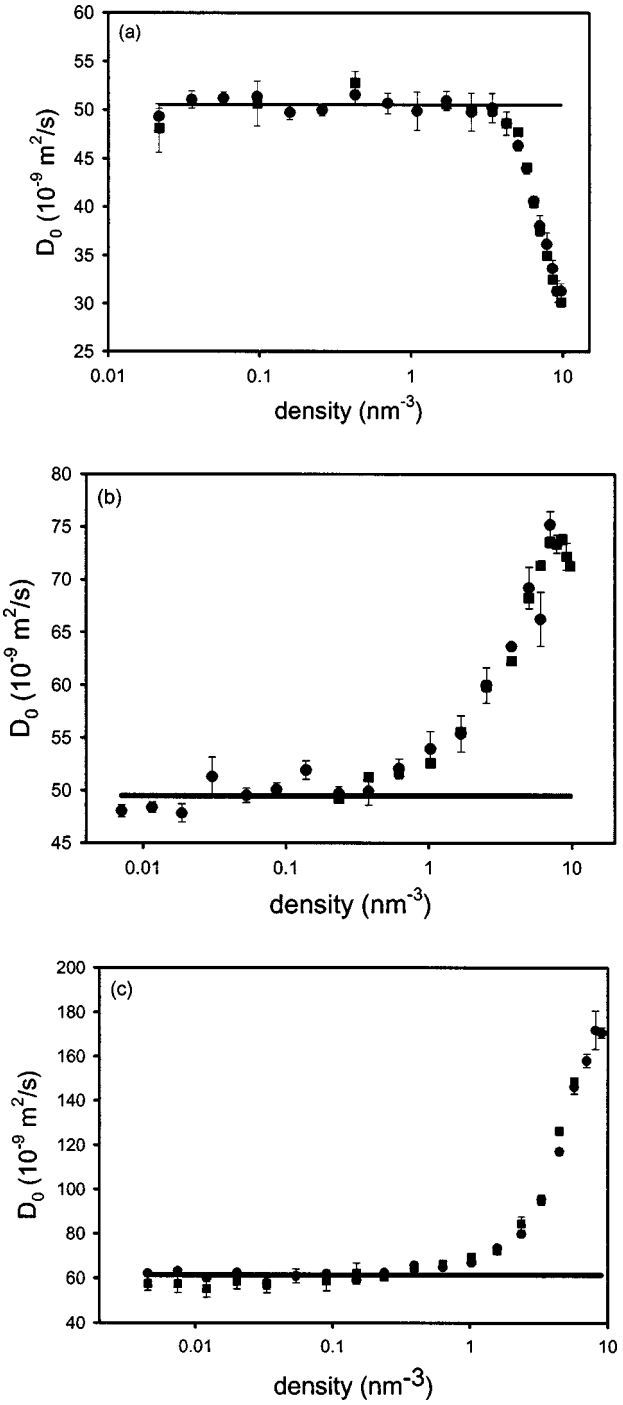

FIG. 4. Density dependence of the transport diffusion coefficient at 298 K, for methane transport in carbon slit pores of width (a) 1.0 nm, (b) 1.4 nm, and (c) 2.0 nm. Data determined from simulation are represented as symbols. Circles represent EMD data, squares show NEMD data. The horizontal lines represent the low-density limit transport diffusion coefficient, predicted by the oscillator model [Eq. (2)].

In transport where viscous effects dominate, it has been observed that the transport coefficient generally increases with density, after a small decrease at transition-regime densities.[1,5,6] This increasing trend has also been observed in methane transport in silica mesopores,[16,17] and the results depicted in Fig. 4 are consistent with these findings, in the wider pores. However, we observe a decreasing trend in D_0, whose onset occurs at lower densities as the pore width is

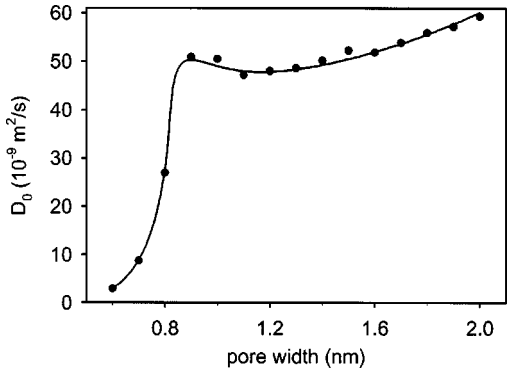

FIG. 5. Variation of transport coefficient with slit width for the adsorption of methane at 300 K in carbon slit pores. The line corresponds to the low-pressure model predictions and symbols to simulation data.

reduced. This decrease of D_0 with increasing density can be interpreted in terms of the effect of the changing fluid structure on the boundary momentum exchange. As the density increases in the narrowest pore, the molecules must arrange themselves in two staggered layers, so that a molecule's neighbors lie on the opposite side of the pore. Consequently, when a molecule changes direction due to a diffuse reflection, and interacts with a neighboring molecule, the neighbor will be driven towards the pore wall. As the density increases, diffuse reflections will thus take place more frequently, and the transport coefficient will decrease. In the wider pores, however, additional layers can form to accommodate molecules, so that a higher pore density is required before effects of this nature are observed. Thus, this mechanism can be used to interpret the upper bound reached in the 1.4 nm and 2.0 nm pores, with the formation of three or four staggered layers. For example, from Fig. 2(b) we estimate that the density of fluid molecules in the central layer reaches approximately 40% of the density of fluid molecules in the outer layers, implying that the staggered arrangement is not universal throughout the whole pore, but is sufficient to affect the overall transport.

B. Oscillator model results

We have used Eq. (2) to obtain estimates of the low-density limit transport diffusion coefficient for methane adsorption in a carbon slit pore at 298 K, in pores ranging in width from 0.6 nm to 2.0 nm. Values of D_0, determined from the model, are plotted in Fig. 5, along with values obtained from NEMD simulation. The NEMD results were obtained from systems at low density, i.e., no greater than 0.1 nm^{-3}. There is excellent agreement between the simulation values and those obtained from the model. We note that each simulation data point requires of the order of 10^7 time steps for satisfactory convergence of the reported value for D_0, which equates to the order of 10^5 s of CPU time per result. By contrast, each value obtained from the model takes of the order of 100 s of CPU time to obtain. Consequently, results obtained from the model represent a significant time saving, and do not contain the statistical errors inherent in molecular dynamics simulations. The model is therefore an attractive alternative means of determining the transport diffusion coefficient.

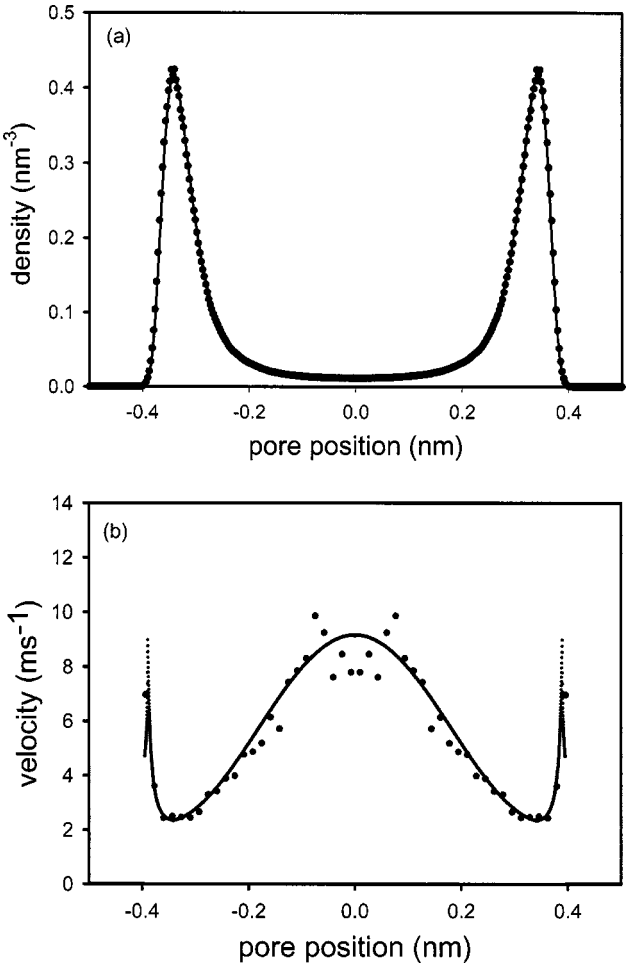

FIG. 6. Comparison of the symmetrized density (a) and velocity (b) profiles predicted by the low density model Eq. (2) and generated by the simulation, for a pore of width 1.4 nm, and driving acceleration of 0.01 nm ps^{-2}.

The density and velocity profiles predicted by the oscillator model are also supported by the NEMD simulation results over the range of systems examined. Figure 6 demonstrates this agreement for the 1.4 nm pore at 298 K. It would therefore appear that the model captures the same essential features of the transport process at low densities that are present in the MD simulations.

In Fig. 7, we show the variation of transport coefficient with temperature, for the four chosen pore widths. At higher temperatures, we observe a near-linear relationship between the transport coefficient and temperature in each pore. Considering Eq. (1), we conclude that the variation of the average velocity of molecules in the pore must vary slowly in this linear region, compared with changes in temperature. We note that, in the limit of infinite temperature, the transport coefficient will approach the value in the limit of a hard solid–fluid interaction, which is infinite for the slit pore. Consequently, the predicted low-density transport coefficients do not admit analysis in accordance with an activated diffusion model, which predicts finite transport coefficients in the infinite temperature limit.

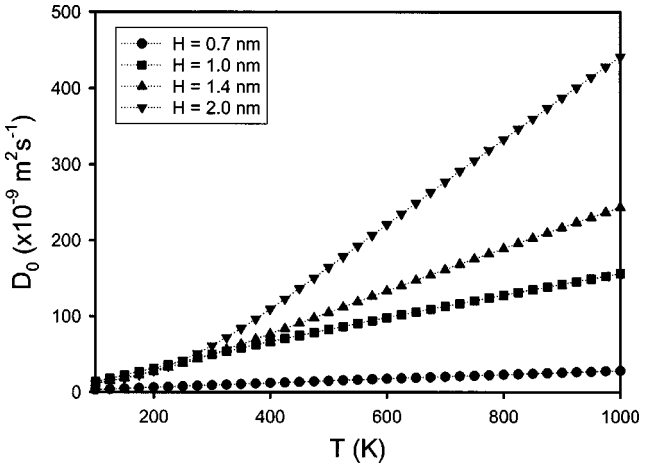

FIG. 7. Variation of transport coefficient with slit width and temperature in the low pressure limit, for methane transport in carbon slit pores. These results indicate that the low-density slit-pore transport coefficients cannot be modelled by an activated diffusion model (see text).

The solid horizontal lines in Fig. 4 depict the value for the transport coefficient predicted by the oscillator model. It is clear from the figure that the oscillator model can be applied over a range of densities corresponding to the Henry's law region, where the solid–fluid interaction dominates intermolecular interactions. At higher densities, the assumptions on which the oscillator model is based are no longer valid, and consequently the model cannot be applied at these densities.

C. Slip flow models

We have evaluated the transport coefficients estimated by the density-dependent models A and B, developed in Sec. II B, over a range of densities, temperatures, and pore sizes, in order to compare with simulation. Figures 8, 9, and 10 show the values of the transport coefficients obtained from these models in the 1.0 nm, 1.4 nm, and 2.0 nm pores at 298 K, 350 K, and 400 K. The figure also shows simulation values of the transport coefficient obtained in the same systems.

We begin our remarks with models B. We recall that model B [Eq. (8)] represents the sum of the low-density limit transport coefficient, determined from the oscillator model, and the viscous term determined from the Navier–Stokes equations. Consequently, we anticipate that it will converge to the correct value at low densities, as is observed in Figs. 8, 9, and 10. Overall, however, we note that model B appears to underestimate the change in the transport coefficient due to an increase in fluid density. The viscous contribution must always be positive, so that the model must fail wherever D_0 is less than the oscillator model prediction. Thus, in the 1.0 nm pore, the decrease in D_0 cannot be accounted for by viscosity contributions alone, and the result is consistent with our interpretation of the upper bound of D_0 in terms of a staggered arrangement of molecules in the pore. The decrease in the transport coefficient can be attributed to the increased rate of diffuse reflections, and it is therefore not surprising that a model that only registers the viscous contribution of this phenomenon will fail to fully predict its effect on the transport coefficient.

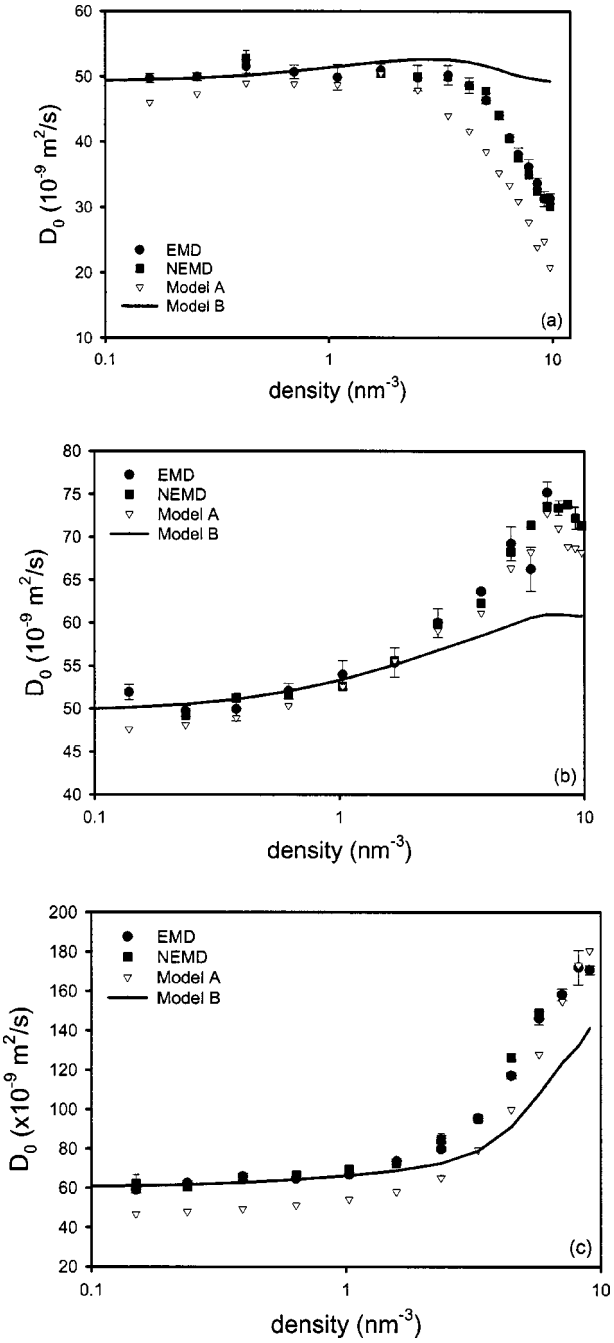

FIG. 8. Estimates of the transport coefficient for transport in the (a) 1.0 nm, (b) 1.4 nm, and (c) 2.0 nm pore at 298 K. The coefficients are determined by EMD (circles) and NEMD (squares) simulation, as well as from model A (triangles) and model B (solid line).

The viscous contribution also experiences a local maximum close to densities where one is observed for the transport coefficient, and appears sufficient to account for the change in D_0 about this maximum in the 1.4 nm pore. This would seem to imply that the boundary contribution has also reached a turning point in this range of densities, indicating the interdependence of the viscous and boundary terms in this region. At higher densities (which already correspond to bulk pressures of the order of 1000 bar) in the 1.4 nm pore,

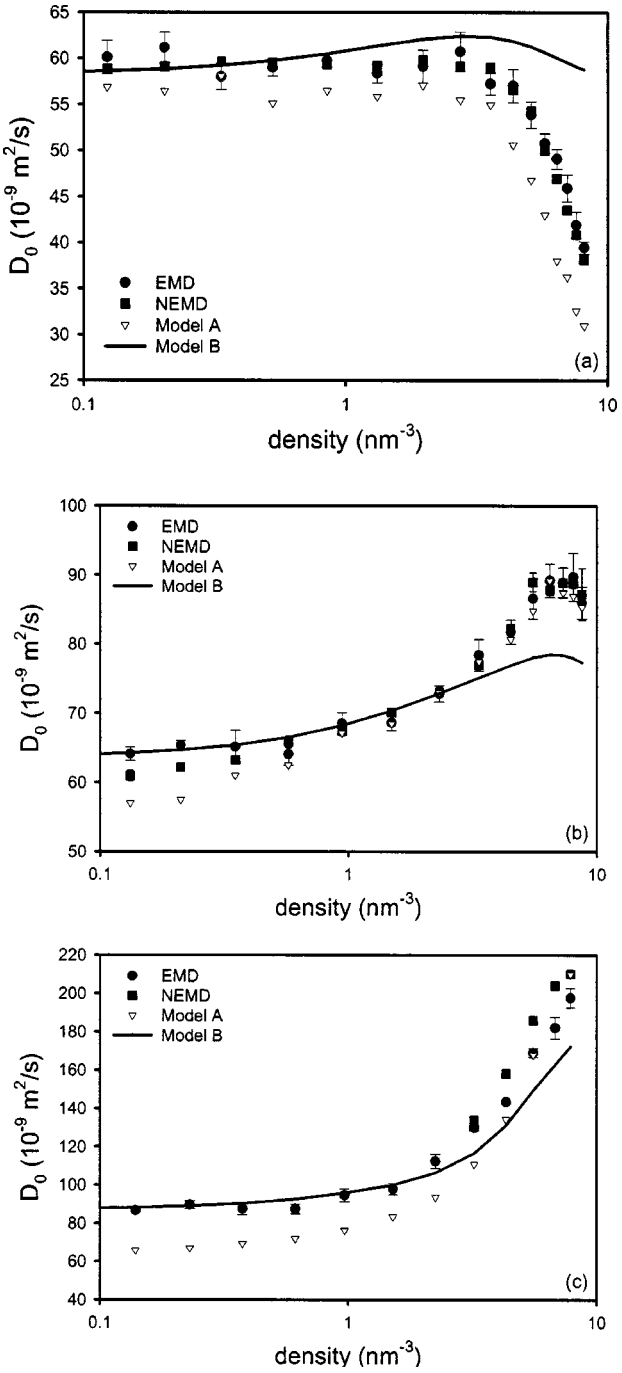

FIG. 9. Estimates of the transport coefficient for transport in the (a) 1.0 nm, (b) 1.4 nm, and (c) 2.0 nm pore at 350 K. The coefficients are determined by EMD (circles) and NEMD (squares) simulation, as well as from model A (triangles) and model B (solid line).

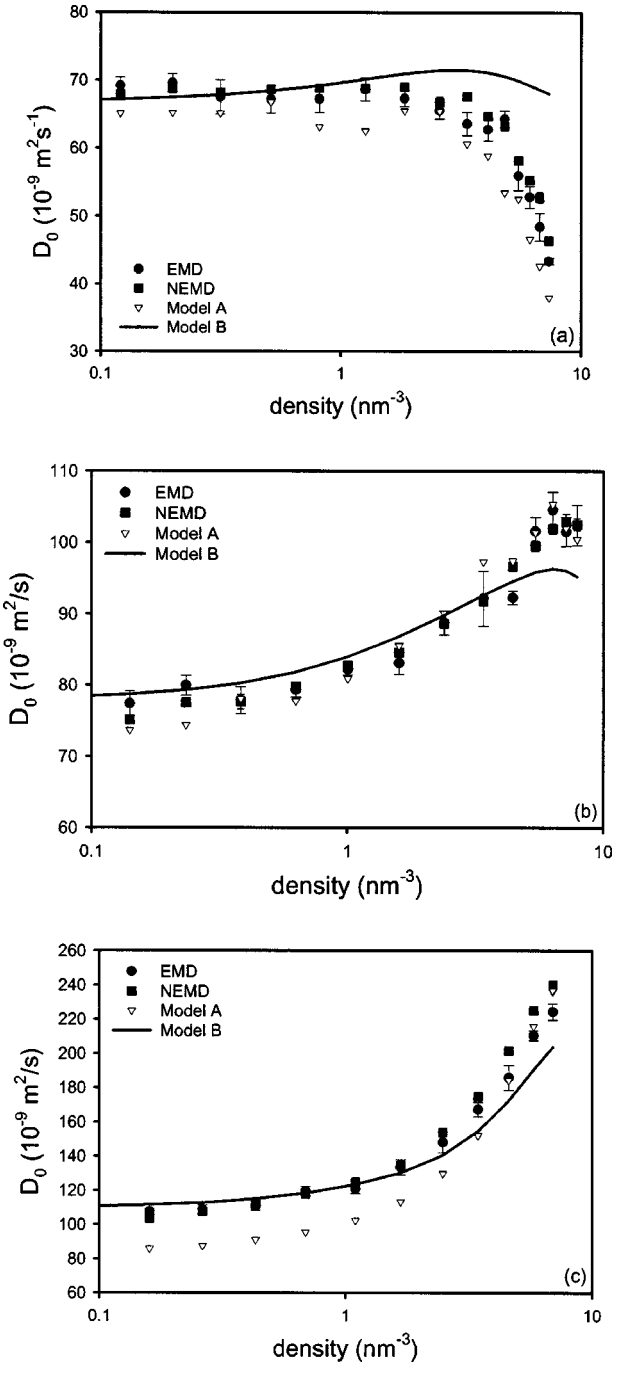

FIG. 10. Estimates of the transport coefficient for transport in the (a) 1.0 nm, (b) 1.4 nm, and (c) 2.0 nm pore at 400 K. The coefficients are determined by EMD (circles) and NEMD (squares) simulation, as well as from model A (triangles) and model B (solid line).

we would anticipate a decrease in D_0 dominated by the boundary term.

We also note that model B appears to become more reliable as the pore width increases. This is consistent with our expectation that, as the pore becomes wider, higher densities are required before boundary effects make a significant contribution to the density-dependence of D_0. Until such densities are reached, we would expect the density-dependence of D_0 to be dominated by changes in the viscous contribution.

While the viscous term in both models is identical, the determination of the boundary terms distinguishes the models. This term is a function of the density profile in model A [Eq. (7)], but is constant in model B. In the 1.0 nm and 1.4 nm pores, the boundary term evaluated by model A is in reasonable agreement with the simulation values. However, this boundary term appears to become less reliable as the pore width increases—in the 2.0 nm pore, it appears to underestimate the simulation results. Overall, we find that model A provides a good prediction of the transport coefficients in the 1.4 nm pore. In the 1.0 nm pore, it appears to overpredict the density-dependent effects, and in the 2.0 nm

pore it appears to underpredict these effects. In all cases, the model correctly predicts the increasing or decreasing trend in the transport coefficient, including in the vicinity of the local maximum observed in the 1.4 nm pore.

Despite its elementary nature, the slip model provides a useful means of estimating transport coefficient behavior, both here and previously.[16,17] The model appears to capture the main features of transport in the micropore, by incorporating a diffusive contribution from momentum exchange at the boundary with a viscous contribution at higher densities. A more sophisticated model of the velocity boundary condition could be developed by considering various aspects of the model in further detail. The frictional boundary condition used in the model assumes a simple kinetic theory model for molecules leaving the repulsive region to interact with the pore wall, and neglects the effect of molecules returning to the system, as well as contributions from the flux in the repulsive region. However, it appears that such effects can be safely neglected in the narrower pores, where the current slip model provides accurate values of the transport coefficient. In the wider pores, the slip model provides a less accurate estimate of the low-density transport coefficient. However, in these regions, model B provides a good alternative model.

We can estimate the Knudsen numbers at which we have applied our model from the kinetic theory expression for the mean free path $\lambda = 1/(\pi\sigma_f^2\rho) \approx 2.2/\rho$ for λ in nm and ρ in nm^{-3}. Consequently, $\mathrm{Kn} \approx 2.2/(\rho H)$ with ρ in nm^{-3} and H in nm. If we consider the limit of applicability of a slip flow model to be governed by the condition $\mathrm{Kn} < 0.1$ accepted in macroscopic pores,[3] we can expect to apply the slip flow model where local densities are of the order of $22/H\ \mathrm{nm}^{-3}$ or higher. In each of the pores, such densities are only reached about the potential maxima beyond the Henry's law region (where the oscillator model is sufficient to estimate the transport coefficient), and in all cases there are regions about the pore center where the local density does not meet this criterion. In such regions, the external confining field will contribute to the shear stress in the fluid—a contribution to the dynamics that is not represented by the constitutive relation $P_{xz} = -\eta(\partial v_z/\partial x)$, and which will therefore not be present in a hydrodynamic model. Due to their low density, we expect the contributions to the flux from these regions to be dominated by the contributions from denser regions where the hydrodynamic theory is expected to hold. However, such low density regions will be a source of discrepancy between the transport coefficients predicted by the models, and those obtained from simulation. The development of models which incorporate these two sources of shear stress in the system—the solid–fluid interaction, and intermolecular interactions—is an area for future research. We note, however, that models A and B provide a useful means of estimating the transport coefficient over a range of Knudsen numbers including the molecular flow, transition, and slip regions.

V. CONCLUSION

We have determined values of the transport diffusion coefficient of methane in microporous carbon for various pore widths and methane densities from EMD and NEMD simulations. In the Henry's law regime, the dynamics are dominated by the solid–fluid interaction, and therefore the oscillator model provides a good estimate of the dynamical and transport behavior. Our simulation results indicate that this regime extends up to densities of the order of 1 nm^{-3}, with corresponding bulk pressures of the order of atmospheric pressure. Consequently, the oscillator model alone may be sufficient to determine the transport properties of many processes which take place in standard laboratory conditions. We note that, in this regime the activated diffusion model does not reflect the underlying diffusion mechanisms, and can only provide an empirical model over narrow ranges of temperature where the coefficient a remains constant. However, the value of a itself is dependent upon the pore size and the temperature range.

At higher densities, where the behavior of the fluid no longer corresponds to the oscillator model, the slip model incorporates the two essential features of diffusive transport—boundary terms which represent the solid–fluid interaction, and viscous terms which represent the fluid–fluid interaction. In the slit micropores, the slip model A provides a useful model for predicting the density-dependent behavior of the transport coefficient. In wider pores, the transport coefficient is not well estimated by the slip model at low densities. However, in these conditions, the sum of the oscillator model transport coefficient and the viscous contribution—model B—can be used as an alternative model, to predict the transport coefficient. The difficulties in applying a single density-dependent model in all pore widths, temperatures, and densities arise from the challenge of incorporating microscopic interactions at the surface within a hydrodynamic theory. It is clear from our results, however, that the hydrodynamic approach provides a promising model from which transport coefficients can be estimated over densities ranging from the molecular flow regime to the slip flow regime.

ACKNOWLEDGMENTS

The authors gratefully acknowledge the financial support of the Australian Research Council under the Discovery Scheme. We also appreciate support and supercomputer access through the Australian Partnership for Advanced Computation and the University of Queensland High Performance Computer Unit. We thank Professor David Nicholson for helpful discussions.

[1] M. Knudsen, Ann. Phys. (Leipzig) **28**, 75 (1909).
[2] M. von Smoluchowski, Ann. Phys. (Leipzig) **33**, 1559 (1910).
[3] A. Beskok, Numer. Heat Transfer, Part B **40**, 451 (2001).
[4] S. L. Thomson and W. R. Owens, Vacuum **25**, 151 (1974).
[5] W. G. Pollard and R. D. Present, Phys. Rev. **73**, 762 (1948).
[6] D. S. Scott and F. A. L. Dullien, AIChE J. **8**, 293 (1962).
[7] H. Grad, Commun. Pure Appl. Math. **2**, 331 (1949).
[8] C. Cercignani and I. Neudachin, Z. Angew. Math. Phys. **30**, 943 (1979).
[9] L. A. Pozhar and K. E. Gubbins, Int. J. Thermophys. **20**, 805 (1999).
[10] H. T. Davis, in *Fundamentals of Inhomogenous Fluids*, edited by D. Henderson (Dekker, New York, 1992).
[11] I. Bitsanis, T. K. Vanderlick, A. Tirrell, and H. T. Davis, J. Chem. Phys. **89**, 3152 (1988).
[12] Y. Zhu and S. Granick, Phys. Rev. Lett. **88**, 106102 (2002).
[13] R. Pit, H. Hervet, and L. Ledger, Phys. Rev. Lett. **85**, 980 (2000).

[14] J.-L. Barret and L. Bocquet, Phys. Rev. Lett. **82**, 4671 (1999).
[15] V. P. Sokhan, D. Nicholson, and N. Quirke, J. Chem. Phys. **115**, 3878 (2001).
[16] S. K. Bhatia and D. Nicholson, Phys. Rev. Lett. **90**, 016105 (2003).
[17] S. K. Bhatia and D. Nicholson, J. Chem. Phys. **119**, 1719 (2003).
[18] D. Nicholson, Carbon **36**, 1511 (1996).
[19] N. A. Seaton, S. P. Friedman, J. M. D. MacElroy, and B. J. Murphy, Langmuir **13**, 1199 (1997).
[20] K. P. Travis, Mol. Phys. **100**, 2317 (2002).
[21] K. P. Travis and K. E. Gubbins, Mol. Simul. **25**, 209 (2000).
[22] G. S. Heffelfinger and F. von Swol, J. Chem. Phys. **100**, 7548 (1994).
[23] J. M. D. MacElroy, J. Chem. Phys. **101**, 5274 (1994).
[24] R. F. Cracknell, D. Nicholson, and N. Quirke, Phys. Rev. Lett. **74**, 2463 (1995).
[25] G. Arya, H.-C. Chang, and E. Maginn, J. Chem. Phys. **115**, 8112 (2001).
[26] D. Nicholson and J. H. Petropoulos, Ber. Bunsenges. Phys. Chem. **79**, 796 (1975).
[27] J. Kärger and D. M. Ruthven, *Diffusion in Zeolites and Other Microporous Solids* (Wiley, New York, 1992).
[28] D. J. Evans and G. P. Morriss, *Statistical Mechanics of Nonequilibrium Liquids* (Academic, London, 1990).
[29] W. A. Steele, *The Interaction of Gases with Solid Surfaces* (Pergamon, Oxford, 1974).
[30] E. J. Maginn, A. T. Bell, and D. N. Theodorou, J. Phys. Chem. **97**, 4173 (1993).
[31] J. C. Maxwell, *Scientific Papers* (Cambridge University Press, Cambridge, 1890), Vol. II, p. 708.
[32] O. J. Jepps, S. K. Bhatia and D. J. Searles Phys. Rev. Lett. **91**, 0126102 (2003).
[33] T. H. Chung, M. Ajlan, L. L. Lee, and K. E. Starling, Ind. Eng. Chem. Res. **27**, 671 (1988).
[34] S. K. Bhatia, O. J. Jepps and D. Nicholson J. Chem. Phys. (in press).
[35] R. F. Cracknell, D. Nicholson, and N. Quirke, Phys. Rev. Lett. **74**, 2463 (1995).